# An iterative adaptive virtual impedance loop for reactive power sharing in islanded meshed microgrids

H. Sellamna [a,b,c], A. Massi Pavan [d], A. Mellit [c,e,*], Josep M. Guerrero [f]

[a] Higher School of Electrical Engineering and Energetic, (ES-GEE), Oran, Algeria
[b] Faculty of Sciences and Technology, Electrical Department, University of Jijel, Algeria
[c] Renewable Energy Laboratory, University of Jijel, Jijel, Algeria
[d] Department of Engineering and Architecture, University of Trieste, Trieste, Italy
[e] The International Center of Theoretical Physics (ICTP), Trieste, Italy
[f] Center for Research on Microgrids CROM, Department of Energy Technology, Aalborg University, Denmark

ARTICLE INFO

*Article history:*
Received 8 June 2020
Received in revised form 29 August 2020
Accepted 2 October 2020
Available online 9 October 2020

*Keywords:*
Islanded meshed micro-grid
Distributed generation
Active and reactive power
Droop control
Iterative virtual impedance

ABSTRACT

This paper proposes a control strategy for the optimization of the reactive power sharing based on an iterative adaptive virtual impedance (IAVI). The IAVI includes two elements: the first is proportional to the reactive power delivered by the distributed generation units at the current iteration, while the second is proportional to the sum of the reactive power variations at the previous iterations. The proposed control strategy has been verified under a Matlab/Simulink environment for an islanded meshed microgrid with three distributed generators. The simulation of different scenarios considering feeder impedance mismatches, different microgrid configurations, and variable loads has shown a good accuracy in the sharing of the reactive power in the microgrid.

The control strategy proposed in this paper can be easily implemented as it does not require any communication link between the generators, any knowledge regarding the feeder impedances, and any local load measurement.

## 1. Introduction

The transition from a centralized to a hybrid centralized/distributed power system concept is due to the high penetration of renewable-based distributed generation (DG) [1]. In this context, microgrids (MGs) were introduced as a very effective configuration for the integration into power systems of the non-dispatchable renewable energy sources (RESs) [2]. In the case of grid-connected MGs, the exchange of active and reactive powers can be imposed by the grid [3,4]. On the contrary, in the case of islanded MGs, the load demand should be properly shared between the different generators operating in the MG [5]. Droop control is often used to regulate active and reactive powers [6] without the use of any external communication link [7].

Whereas the sharing of active power is usually easy to achieve as all the DGs work at the same frequency, the regulation of the reactive power sharing is more complicated because of the different voltage of the DGs due to the difference in the impedances of the feeders [7]. Different droop control-based regulators have been developed and presented in the literature [8]. In [9] a "Q-V dot droop" method is proposed to improve the sharing of the reactive power. In [10] the injection of small real power disturbances is used to estimate the reactive power control error. Different methods based on the estimation of the impedance lines are presented in [11] and [12]. Secondary droop control has been used in [13–15] in order to eliminate the reactive power sharing error by compensating the voltage level. A virtual Impedance (VI) method has been widely used with good results in many applications including reactive power sharing in MGs [16,17] and improvement of the power control stability [18].

The VI approach used in [19] differs from traditional methods because of its capability to prevent high harmonics content. In [20] a virtual harmonic impedance has been developed to control the harmonic power sharing in an islanded MG. Virtual impedance-based controllers have been presented in [21,22]. In [23] an Adaptive Virtual Impedance (AVI) based on the integration of the voltage drop between different distributed generators is proposed. In [24] the authors introduced a proper inductance in order to improve the reactive power sharing by estimating the feeder impedances. In [25] and [26] the voltage is compensated by a secondary controller that optimizes the reactive power sharing. In this case, the knowledge of the voltage at the Point of Common Coupling (PCC) is required. A comprehensive review showing the advantages and the limits of the most common control methods used for the reactive power sharing in islanding MGs can be found in [27].

* Corresponding author at: Renewable Energy Laboratory, University of Jijel, Jijel, Algeria.
*E-mail address:* amellit@ictp.it (A. Mellit).

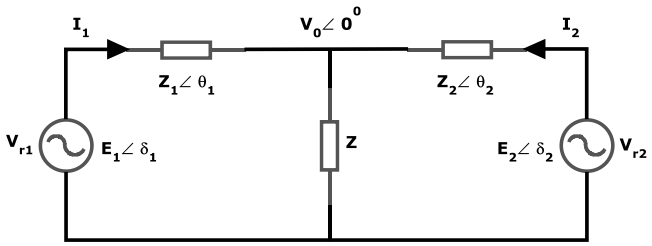


**Fig. 1.** Two generators feeding a common load.

It is worth mentioning that the most of the aforementioned methods have been developed based on a classical MG structure where the reactive power sharing is related only to the feeders impedance mismatch.

In this paper, a new control strategy named Iterative Adaptive Virtual Impedance (IAVI) is presented. The IAVI is adjusted considering two contributes: the first is proportional to the reactive power at the previous iterations, while the second is proportional to the sum of the reactive power variations at the previous iterations. The investigated islanded meshed MG consists of three parallel-connected distributed generators. The share of the reactive power in the MG has been evaluated considering two different control techniques: the first one is based on a simple droop control, while the second uses a droop control virtual impedance. The controllers have been developed without the use of any communication link between the different DG units. The performance of the proposed control strategy has been compared with the well known droopless technique [18].

The rest of the paper is organized as follows: Section 2 describes the use of the conventional droop control. To eliminate the reactive power inaccuracy, an analysis based on reactive power sharing without and with virtual impedances is presented in Section 3. The proposed IAVI control strategy, stability analyses, controller parameters setting, and controller synchronizations are provided in Section 4. The results are presented and discussed in Section 5.

## 2. Droop control

Active power–frequency ( P–f) and reactive power–voltage ( Q–V) droop-based control techniques have been effectively applied in MGs to control the share of active and reactive powers [7, 12]. These methods have been widely used because they are simple and they do not require any communication link between the generators operating in the MG.

Fig. 1 shows a microgrid with two generators feeding a common load. The currents produced by the two generators are:

$$I_i = \frac{E_i\angle\delta_i - V_0\angle 0^0}{Z_i\angle\theta_i} = \frac{E_i\cos\delta_i - V_0 + jE_i\sin\delta_i}{Z_i\angle\theta_i} \quad i = 1, 2 \tag{1}$$

Where $E_i$ and $\delta_i$ are the voltage amplitude and angle of $i$th generator, $Z_i$ and $\theta_i$ the module and the phase of the $i$th feeder impedance, and $V_0$ is the PCC voltage.

The active and reactive powers can be calculated as [4,18]:

$$P_i = \left(\frac{E_i \times V_0}{Z_i\angle\theta_i}\cos\delta_i - \frac{V_0^2}{Z_i\angle\theta_i}\right)\cos\theta_i + \frac{E_i \times V_0}{Z_i\angle\theta_i}\sin\delta_i\cos\theta_i \tag{2}$$

$$Q_i = \left(\frac{E_i \times V_0}{Z_i\angle\theta_i}\cos\delta_i - \frac{V_0^2}{Z_i\angle\theta_i}\right)\sin\theta_i + \frac{E_i \times V_0}{Z_i\angle\theta_i}\sin\delta_i\sin\theta_i \tag{3}$$

If the feeder impedance is purely inductive, then Eq. (2) and Eq. (3) can be written as:

$$Q_i = \left(\frac{E_i \times V_0}{x_{mi}}\mathrm{Cos}\delta_i - \frac{V_0^2}{x_{mi}}\right) \tag{4}$$

$$P_i = \frac{E_i \times V_0}{x_{mi}}\mathrm{Sin}\,(\delta_i) \tag{5}$$

Where $x_{mi}$ is the feeder reactance.

When $\delta_i$ is small, then the active and the reactive powers can be expressed as [4]:

$$Q_i \approx \frac{E_i \times V_0 - V_0^2}{x_{mi}} \tag{6}$$

$$P_i \approx \frac{E_i \times V_0}{x_{mi}}\delta_i \tag{7}$$

Eqs. (6) and (7) represent the base of the droop control method and show that the reactive power can be set by varying the output voltage magnitude, while the active power can be adjusted varying the voltage frequency being the generator angle a function of the frequency.

Fig. 2 shows the relationships between the frequency and the active power, and the one between the reactive power and the voltage magnitude. These relationships can be expressed as follows [4,18,24]:

$$\omega = \omega_n - n \times P \tag{8}$$

$$E = E_0 - m \times Q \tag{9}$$

Where $\omega$ and $\omega_n$ are the reference and the nominal frequency, $E$ and $E_0$ are the reference and the nominal voltage, $m$ and $n$ the active and the reactive droop slopes.

When the MG operates in a stable region, the generators work synchronously and the sharing of real power is accurate. On the contrary, there is no reference for the sharing of the reactive power because the voltage of the generators can be different due to the line impedances mismatch.

In order to achieve an accurate reactive power sharing, the line impedances must be modified to be inversely proportional to both the reactive power rating and the sum of the reactive power variation.

## 3. Reactive power sharing analysis

### 3.1. Conventional droop control

Fig. 3 shows a meshed MG with two generators with the same nominal power operating in an islanded mode. Each generator feeds both a local and two common loads. The relationships between the DGs voltages and their reactive power is given by:

$$E_1 = E_0 - m \times Q_1 \tag{10}$$

$$E_2 = E_0 - m \times Q_2 \tag{11}$$

If the resistive parts of the feeder impedances are negligible, then the voltage drops have to be smaller than the 5% of the nominal voltage (i.e., $E_0 \cong E_1$) in order to avoid system instabilities [16]. The voltage drops are given by [16]:

$$E_1 - V_{N1} = \frac{X_1(Q_1 - Q_{LL1})}{E_0} \tag{12}$$

$$E_2 - V_{N2} = \frac{X_2(Q_2 - Q_{LL2})}{E_0} \tag{13}$$

Where $V_{N1}$ and $V_{N2}$ are the voltages corresponding to the local load nodes, while $Q_{LL1}$ and $Q_{LL2}$ are the local loads reactive powers.

The reactive powers through the nodes $N_1$ and $N_2$ are:

$$Q_{N1} = -Q_{N2} = Q_1 - Q_{LL1} - Q_{CL1} = -Q_2 + Q_{LL2} + Q_{CL2} \tag{14}$$

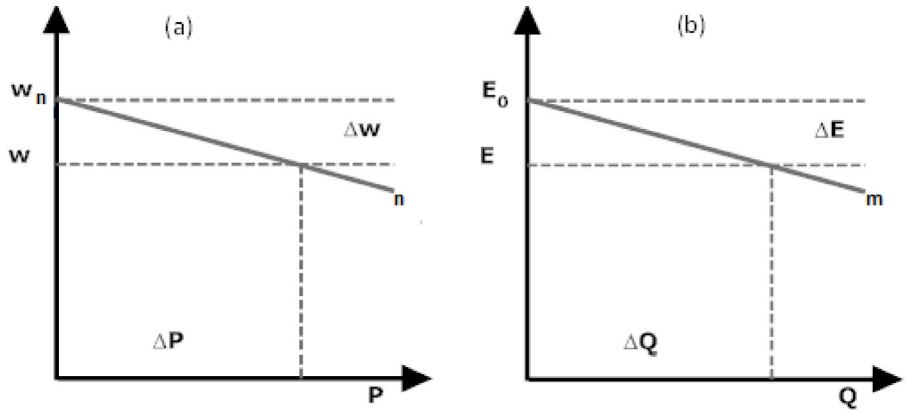


**Fig. 2.** Droop characteristics: (a) active power–frequency, (b) reactive power–voltage..

Where $Q_{CL1}$ and $Q_{CL2}$ are the reactive powers related to the common loads.

The voltage drop caused by $X_{12}$ is:

$$V_{N2} - V_{N1} = \frac{X_{12}(Q_2 - Q_{LL2} - Q_{CL2})}{E_0} \tag{15}$$

Using equations from 10 to 15, the voltage drops between the generators and node $N_1$ are:

$$E_1 - V_{N1} = \frac{X_1(1-a_1)}{E_0} Q_1 \tag{16}$$

$$E_2 - V_{N1} = \frac{X_2\,(1-a_2) + X_{12}\,(1-b_2)}{E_0} Q_2 \tag{17}$$

Where $a_1$, $a_2$, $b_1$ and $b_2$ have been defined as:

$$a_1 = \frac{Q_{LL1}}{Q_1} \tag{18}$$

$$a_2 = \frac{Q_{LL2}}{Q_2} \tag{19}$$

$$b_1 = \frac{Q_{CL1}}{Q_1} \tag{20}$$

$$b_2 = \frac{Q_{CL2}}{Q_2} \tag{21}$$

By means of Eqs. (20) and (21), the considered microgrid can be modelled using a classical structure as shown in Fig. 4. In this case, the PCC corresponds to node $N_1$ and the line impedances are a function of the reactive power demand.

The total reactive power load demand can be expressed as follows:

$$Q_{TOT} = Q_1 + Q_2 = Q_{LL1} + Q_{CL1} + Q_{LL2} + Q_{CL2} \tag{22}$$

The equivalent line impedances of the equivalent model are:

$$X_1\,(Q) = X_1\,(1-a_1) \tag{23}$$

$$X_2\,(Q) = X_2\,(1-a_2) + X_{12}\,(1-b_2) \tag{24}$$

Using Eqs. (20)–(22), the reactive power accuracy error can be expressed as:

$$\begin{aligned} \Delta Q &= \frac{1}{2} Q_{TOT} - Q_1 \\ &= \frac{X_1\,(1-a_1) - X_2\,(1-a_2) - X_{12}\,(1-b_2)}{2E_0 m + X_1\,(1-a_1) - X_2\,(1-a_2) + X_{12}\,(1-b_2)} \end{aligned} \tag{25}$$

Considering now Eqs. (23) and (24), the reactive power accuracy error is given by:

$$\Delta Q = \frac{X_1(Q) - X_2\,(Q)}{2E_0 m + X_1\,(Q) + X_2\,(Q)} Q_{TOT} \tag{26}$$

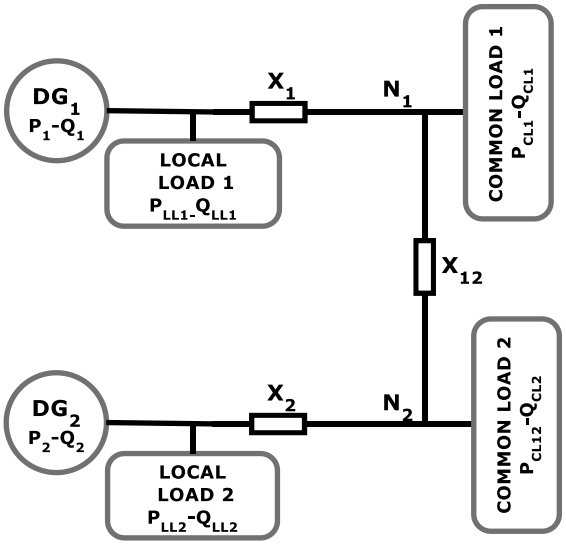


**Fig. 3.** A meshed microgrid with two generators.

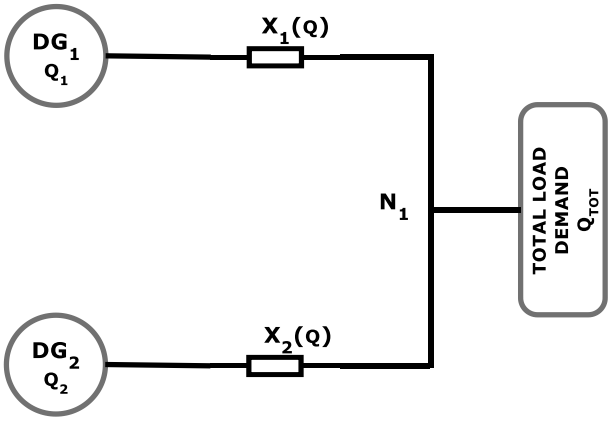


**Fig. 4.** Equivalent model of the meshed microgrid with two generators.

Eqs. (25) and (26) show that the reactive power sharing error depends on the feeder impedances, the local loads reactive power, the total reactive power, and the structure of the microgrid. Eq. (26) also shows that the reactive power sharing accuracy can be achieved both by increasing the equivalent feeder impedances, and by reducing the equivalent feeder impedances mismatch. The first approach might lead to large frequency and

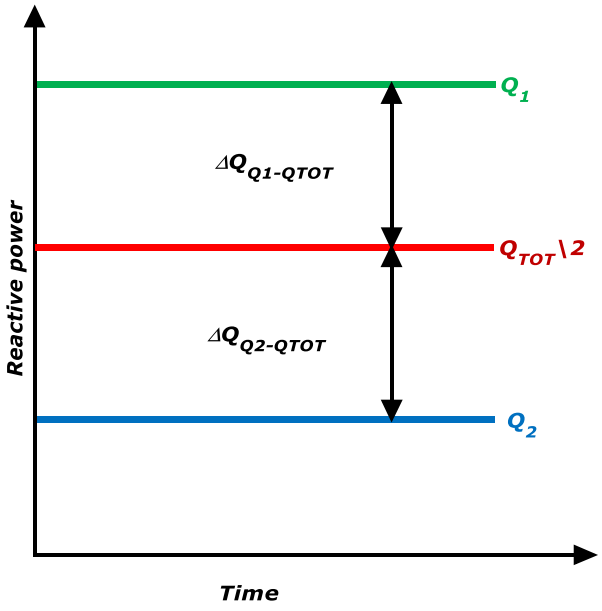


**Fig. 5.** Reactive power sharing error.

voltage deviations affecting the system stability (the condition for the stability is $\Delta V < 5\%E_0$) and for this reason the second approach is preferred.

### 3.2. Virtual impedance

For a microgrid with two distributed generators, the reactive power can be expressed as a function of the total load demand:

$$Q_1 = \frac{1}{2}Q_{TOT} - \Delta Q_{Q-Q_{TOT}} \tag{27}$$

$$Q_2 = \frac{1}{2}Q_{TOT} + \Delta Q_{Q-Q_{TOT}} \tag{28}$$

With reference to Fig. 5, $\Delta Q_{Q-QTOT}$ is the error in the reactive power that, based on Eqs. (18)–(20), can be expressed as:

$$\Delta Q_{Q-Q_{TOT}} = \frac{X_1(Q) - X_2(Q)}{2E_0 m + X_1(Q) + X_2(Q)} Q_{TOT} \tag{29}$$

When the total reactive power load demand is constant and the reactive droop slope is small, Eq. (29) becomes:

$$\Delta Q_{Q-Q_{TOT}}{}^0 = \frac{X_1(Q) - X_2(Q)}{X_1(Q) + X_2(Q)} Q_{TOT} \tag{30}$$

Where $\Delta Q^0_{qi-QTOT}$ is the reactive power sharing error at time $t = 0$.

The feeder impedances mismatch can then be written as:

$$X_1(Q) - X_2(Q) = (X_1(Q) + X_2(Q)) \times \frac{\Delta Q_{Q-Q_{TOT}}{}^0}{Q_{TOT}} \tag{31}$$

If at time $t = T_1$ (i.e. during iteration 1) we connect a virtual impedance, then the reactive power sharing error becomes:

$$\Delta Q_{Q-Q_{TOT}}{}^{T1} = \frac{X_1(Q) - X_2(Q) + X_{v1} - X_{v2}}{X_1(Q) + X_2(Q) + X_{v1} + X_{v2}} Q_{TOT} \tag{32}$$

Where $\Delta Q^{T1}_{Q-QTOT}$, $Xv_1$, and $Xv_2$ are the reactive power sharing error at time $t = T_1$, the virtual impedances of DG1, and the one of DG2 respectively.

The reactive power sharing is accurate when $\Delta Q^{T1}_{Q-QTOT} = 0$, and this corresponds to the feeder impedances mismatch given by:

$$X_1(Q) - X_2(Q) = -X_{v1} + X_{v2} \tag{33}$$

Based on Eqs. (31) and (33), the virtual impedances can be calculated as:

$$-X_{v1} + X_{v2} = -(X_1(Q) + X_2(Q)) \times \frac{\Delta Q_{Q-Q_{TOT}}{}^0}{Q_{TOT}} \tag{34}$$

Eq. (34) can be rewritten as:

$$-X_{v1} + X_{v2} = -\frac{1}{2}\left(\frac{X_1(Q)}{Q_1} + \frac{X_2(Q)}{Q_2}\right)\Delta Q_{Q-Q_{TOT}}{}^0 \tag{35}$$

Thus, for an accurate reactive power sharing, the virtual impedances should be proportional to the reactive power sharing error as follows:

$$X_{v1} = \frac{X_1(Q)}{2.Q_1}\Delta Q_{Q-Q_{TOT}}{}^0 \tag{36}$$

$$X_{v2} = -\frac{X_2(Q)}{2.Q_2}.\Delta Q_{Q-Q_{TOT}}{}^0 \tag{37}$$

## 4. The IAVI controller

In this section, the proposed controller based on the iterative adaptive virtual impedance control strategy is presented. As shown in Fig. 6, the controller is made of three stages. The first stage (named droop control) is used to generate the reference voltage based on the indirect measurement of active and reactive powers. The second stage consists of two control loops, one for the voltage and one for the current. The IAVI controller with its output $\left(Xv_i^n\right)$ represents the third stage. The virtual impedance is adjusted periodically at each time step and, at the iteration number $n$, the adaptive virtual impedance of the $i$th distributed generator of the microgrid is:

$$X_{Vi}{}^n = k_1 \times Q_i^{n-1} - k_2 \times \sum_{j=1}^{n-1} \frac{\Delta Q_i{}^j}{Q_i{}^j} \tag{38}$$

Where $\Delta Q_i^j$ is the reactive power variation at the iteration number $j$, while $k_1$ and $k_2$ are two parameters used to regulate the feeder impedances.

With reference to Fig. 7, a large variation of reactive power corresponds to a small variation of the generator impedance and vice versa.

As an example, we now consider a microgrid with two generators a constant reactive power load demand, and the possibility to vary the reactive power produced by the generators. With reference to Eq. (38), a positive reactive power variation $(k_1 \times Q_i^{n-1})$ corresponds to the larger production of reactive power and vice versa. This fact is used in order to cancel the feeder impedances mismatch and achieve a perfect reactive power sharing as shown in Fig. 8.

The iterative virtual impedance at the iteration number $n+1$ is:

$$X_{Vi}{}^{n+1} = k_1 \times Q_{DGi}{}^n - k_2 \times \sum_{j=1}^{n} \frac{\Delta Q_{DGi}{}^j}{Q_{DGi}{}^j} \tag{39}$$

From Eqs. (38) and (39), the variation of the adaptive virtual impedance in two successive iterations is:

$$X_{Vi}{}^{n+1} - X_{Vi}{}^n = k_1 \times \Delta Q_{DGi}{}^n - k_2 \times \frac{\Delta Q_{DGi}{}^n}{Q_{DGi}{}^n} \tag{40}$$

$$\Delta X_{Vi}{}^{n+1} = \left(k_1 - k_2 \times \frac{1}{Q_{DGi}{}^n}\right) \times \Delta Q_{DGi}{}^n \tag{41}$$

Then, the variation of the iterative adaptive virtual impedance and of the reactive power change are opposite only if:

$$k_1 < \frac{k_2}{Q_{MAX}} \tag{42}$$

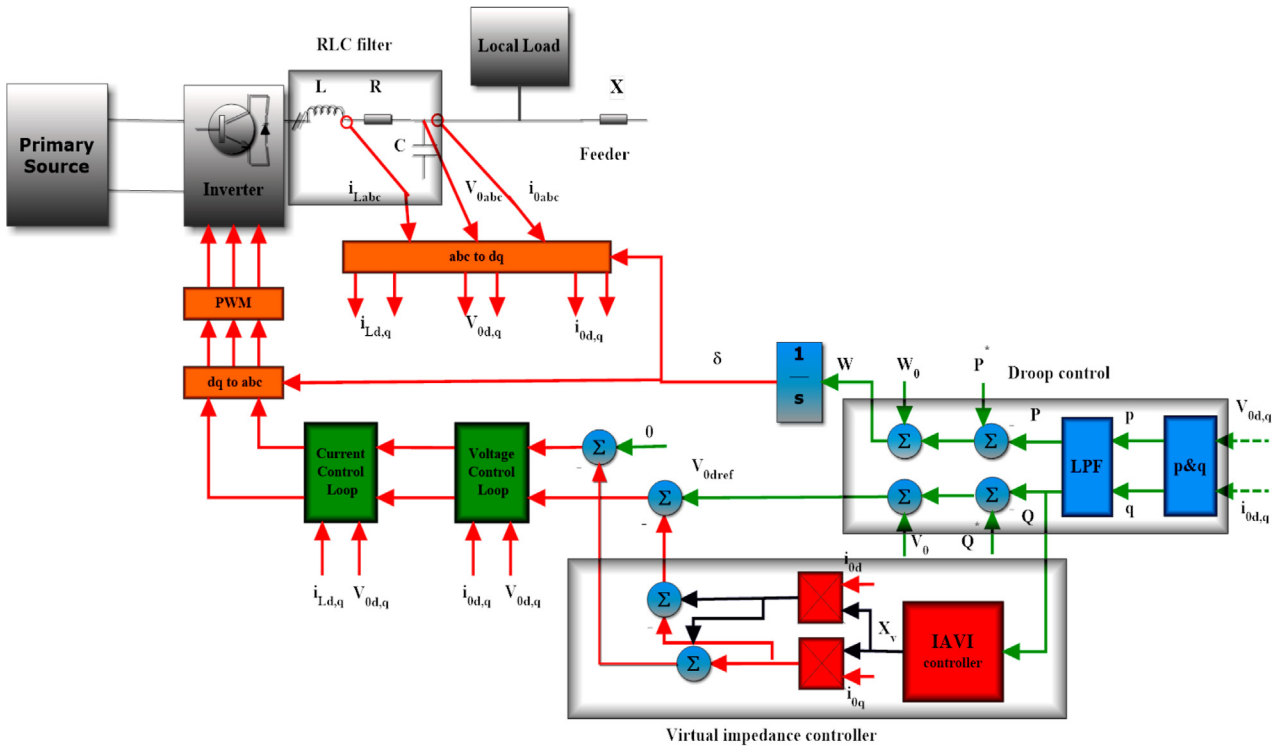


**Fig. 6.** The whole proposed generator controller.

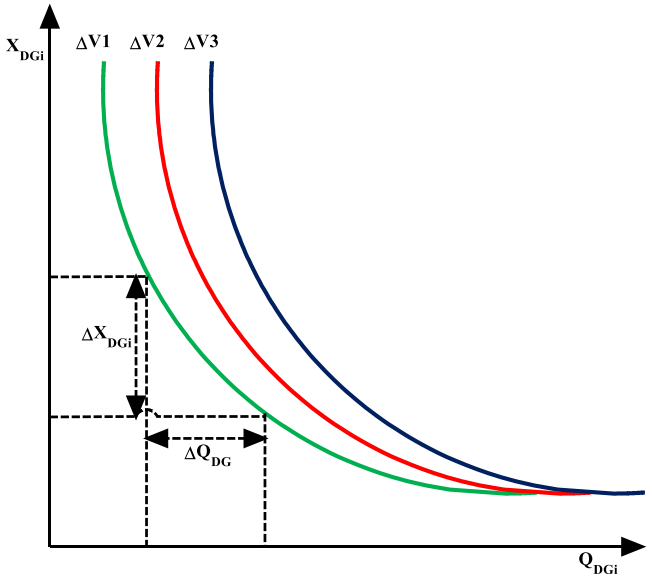


**Fig. 7.** Virtual impedance — reactive power characteristics.

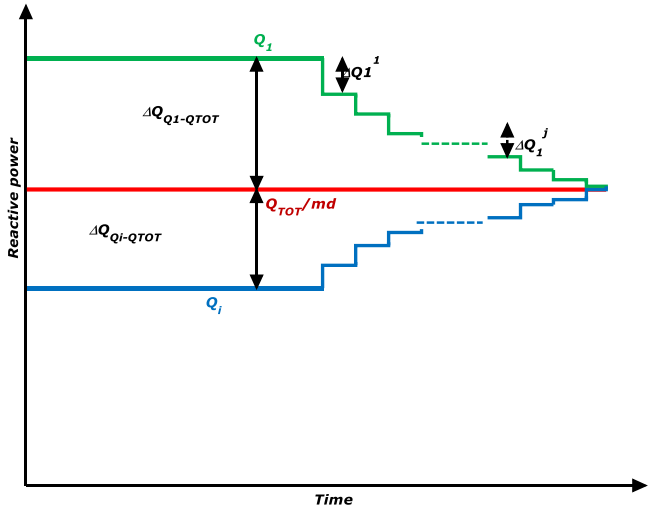


**Fig. 8.** Reactive power regulation in a microgrid with two generators.

### 4.1. Small signal stability

In order to assess the stability of the microgrid as a function of the coefficients $k_1$ and $k_2$, in this section we introduce the small-signal model of the considered system. In the case of grid-forming inverters that is the case of the present study, a reactive power control loop is indispensable [28,29].

The active and reactive powers exchange between a distributed generator DG and a node $N$ can be expressed as:

$$P = \frac{V_{DG}V_N \mathrm{Sin}(\delta)}{X + X_V} - P_{LL} \tag{43}$$

$$Q = \frac{({V_{DG}}^2 + V_{DG}.V_N \mathrm{Cos}\,(\delta))}{X + X_V} - Q_{LL} \tag{44}$$

Where $X$ and $X_V$ are the feeder and the virtual impedances, $P_{LL}$ and $Q_{LL}$ the local load active and reactive powers, $\delta$ is the power angle, $V_{DG}$ and $V_N$ the generator and node voltages.

Table 1 lists the parameters used for the considered system.

From Eq. (38), the virtual impedance can is:

$$\Delta Q_i^j = \Delta {Q_{Q-Q_{TOT}}}^0 - ({Q_{DGi}}^{n-1} - Q^*) \tag{45}$$

$$X_V \simeq k_1 \times Q - k_2 \times \frac{1}{s} \times \frac{\Delta {Q_{Q-Q_{TOT}}}^0 - (Q - Q^*)}{Q} \tag{46}$$

Where $Q^*$ is the desired power sharing.

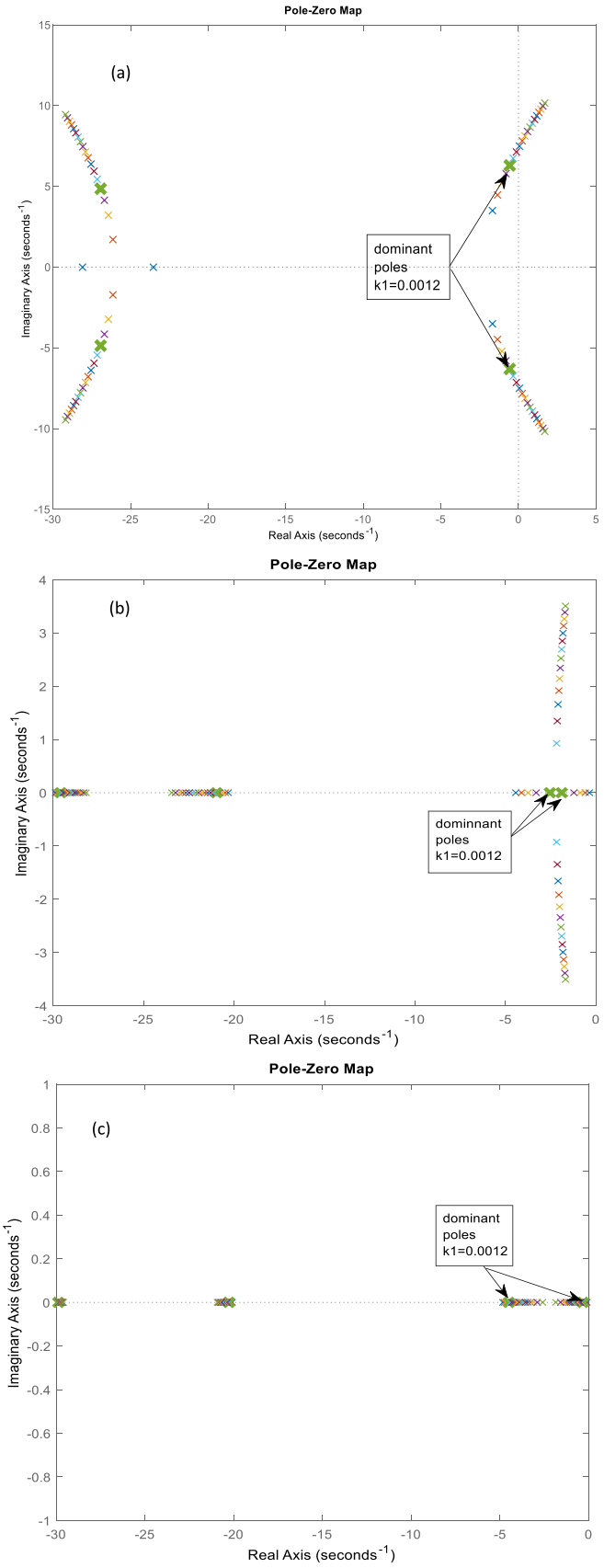


**Fig. 9.** Root trajectories of the characteristic equation: (a) $\tau$ = 0.1 s/VAR, (b) $\tau$ = 0.2 s/VAR, and (c) $\tau$ = 0 s/VAR.

**Table 1**
System parameters.

| Description | Parameter | Value |
|---|---|---|
| Nominal voltage | $E_0$ | 220 V |
| Filter | $R$, $L$, $C$ | 0.5 Ω, 5 mH, 75 nF |
| Switching frequency | $f_s$ | 20 kHz |
| Frequency droop coefficient | $n$ | 0.002 rad/(W) |
| Voltage droop coefficient | $m$ | 0.0035 V/VAR |
| Voltage loop gains | $K_{pv}$, $K_{iv}$ | 5500 |
| Current loop gains | $K_{pi}$, $K_{ii}$ | 1.5, 100 |
| Low pass filter frequency | $W_0$ | 314 rad/s |

If we define $\tau = k_1/k_2$, then $X_V$ can be expressed as:

$$X_V \simeq \tau \times Q - \frac{1}{s} \times \frac{\Delta Q_{Q-Q_{TOT}}{}^{0} - (Q - Q^*)}{Q} \tag{47}$$

Linearizing Eqs. (43), (44) and (47) around the operating point, we obtain:

$$\Delta P = a_{vp} \times \Delta V_{DG} + a_{\delta p} \times \Delta\delta + a_{xp} \times \Delta X_V \tag{48}$$

$$\Delta Q = a_{vq} \times \Delta V_{DG} + a_{xq} \times \Delta X_V \tag{49}$$

$$\Delta X_V = k_1\left(1 - \tau\frac{k}{s}\right) \times \Delta Q \tag{50}$$

Where the coefficients $a_{vp}$, $a_{\delta p}$, $a_{xp}$, $a_{vq}$, $a_{xq}$ and $k_1$ are calculated around the previous operating point.

Because of the low-pass filter, the power angle and the variations in the output generator voltage can be expressed as:

$$\Delta\delta = \frac{-m.w_0}{s(s + w_0)}\Delta P \tag{51}$$

$$\Delta V = \frac{-n.w_0}{s + w_0}\Delta Q \tag{52}$$

Using equations from (48) to (52), the system can then be described using the following characteristic equation

$$a_{C0} + a_{C1}s + a_{C2}s^2 + a_{C3}s^3 + a_{C4}s^4 = 0 \tag{53}$$

Where the system characteristic equation coefficients are:

$$a_{C0} = -2kk_1m\tau\, w_0{}^2(a_{xp} - a_{\delta p}a_{xq}) \tag{54}$$

$$a_{C1} = w_0{}^2\left(a_{vp}mn + a_{\delta p}m\left(a_{vq}n + a_{xq}k_1\left(k\tau + w_0\right)\right) - a_{xp}m\frac{k_1}{w_0}\left(k\tau + w_0\right) + a_{xq}kk_1\tau\right) \tag{55}$$

$$a_{C2} = w_0\left(a_{\delta p}m\left(a_{xq}k_1 + 1\right) - a_{xp}mk_1 + a_{vq}nw_0 + 2a_{xq}k_1k\tau + a_{xq}k_1w_0 + w_0\right) \tag{56}$$

$$a_{C3} = w_0\left(a_{vq}n + 2\right) + a_{xq}k_1(2w_0 + k\tau) \tag{57}$$

$$a_{C4} = a_{xq}k_1 + 1 \tag{58}$$

Based on Eq. (53), Fig. 9 shows the influence of the controller parameters $k_1$ and $\tau$ on the system stability, rapidity and precision.

Fig. 9 shows that for larger $\tau$, the dominant poles move away from the imaginary axis resulting in a fast dynamic response and good stability of the system. On the other hand, in order to eliminate the effect of the sampling, the speed of the controller has to be not too fast. Thus, in order to eliminate the effect of the sampling period without affecting the system stability, $\tau$ is set to 0.2 s/VAR. The coefficient $k_1$ is set to 0.0012 so that the dominant poles are purely real. In this way, there are no oscillations in the reactive power sharing and the condition of convergence given by Eq. (42) is verified.

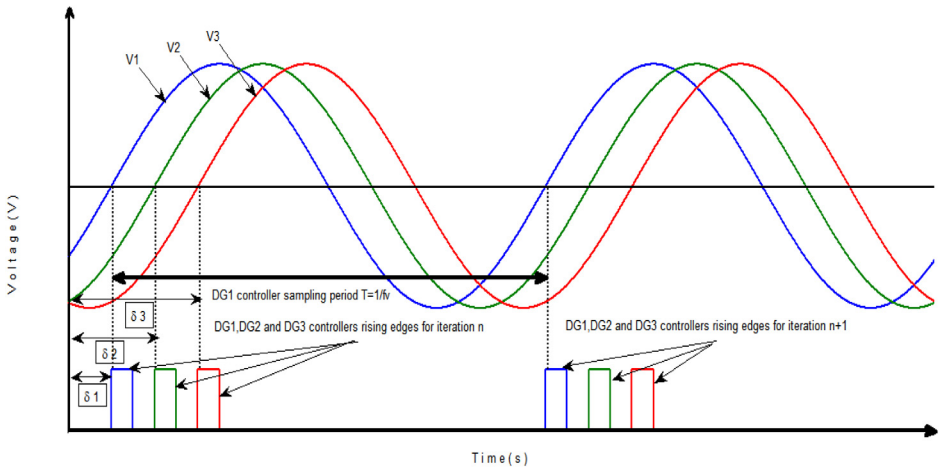


**Fig. 10.** Synchronization of the generator controllers.

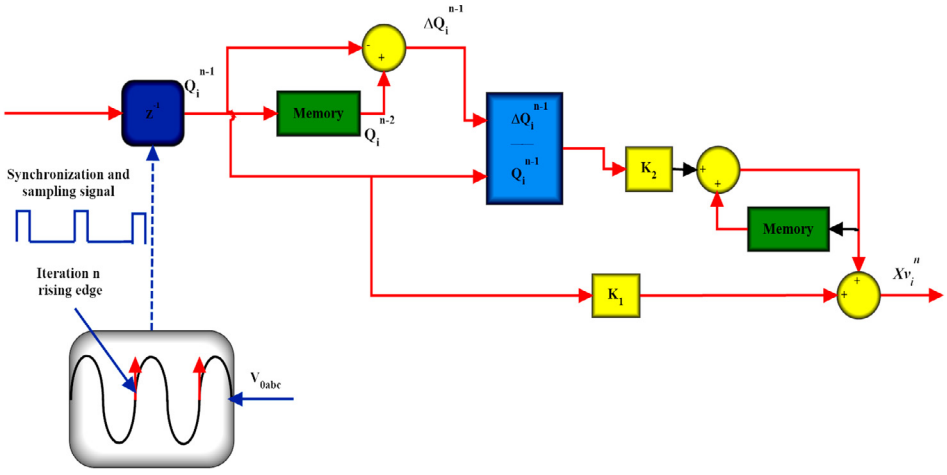


**Fig. 11.** The proposed IAVI controller.

### *4.2. Synchronization and sampling period*

The proposed technique works iteratively with the sampling period $T$, while the controllers of each generator must operate synchronously without the use of any communication link. When the period $T$ starts, the controllers receive the values of the reactive power at times $T$ and $(T+1)$, and calculate the value of the virtual impedances according to equation 38. Nevertheless, the major problem is how to synchronize the controllers without any communication link.

As shown in Fig. 10, the generators in the microgrid operate at the same frequency $f_v$. Due to the fact that the three power angles $\delta_1$, $\delta_2$ and $\delta_3$ are very small if related with the pulsation of the low-pass filter and with the one of the generator voltages then these can be assumed synchronized.

With reference to Fig. 10, in order to synchronize the three controllers in the microgrid, the iteration rising edge time of these controllers must be synchronized. The sampling period $T$ is then set to the same value as the period of the output voltage so that the effect of the power angle on the controllers synchronization can be eliminated. This choice also allows tracking the rapid variations in the load demand, and ensures a reliable measure of the reactive power variation since the period $T$ is similar to the low-pass filter time constant.

## 5. Results and discussion

In order to verify the performance of the IAVI controller depicted in Fig. 11, the meshed microgrid with three distributed generators shown in Fig. 12 has been considered.

The performance of the developed controller has been simulated in a Matlab/Simulink environment for the following three case studies:

(1) Case study 1: The power demand is kept constant, while the structure of the microgrid together with the parameters of the IAVI controller are kept fixed;

(2) Case study 2: The power demand is variable, and the structure of the microgrid is flexible. Again, the parameters of the IAVI controller are kept fixed;

(3) Case study 3: As in the first case study, the power demand is kept constant and the structure of the microgrid is kept fixed. In this case, the performance of the IAVI controller is assessed using different adaptation coefficients.

### *5.1. Case study 1*

In the first case study, the performance of the IAVI controller has been compared with the one of a traditional droopless controller. This latter has a reference virtual impedance equal to 0.5 Ω and ad adaptation coefficient equal to 0.0024. As shown in Fig. 12, the three feeder impedances have different values. In this

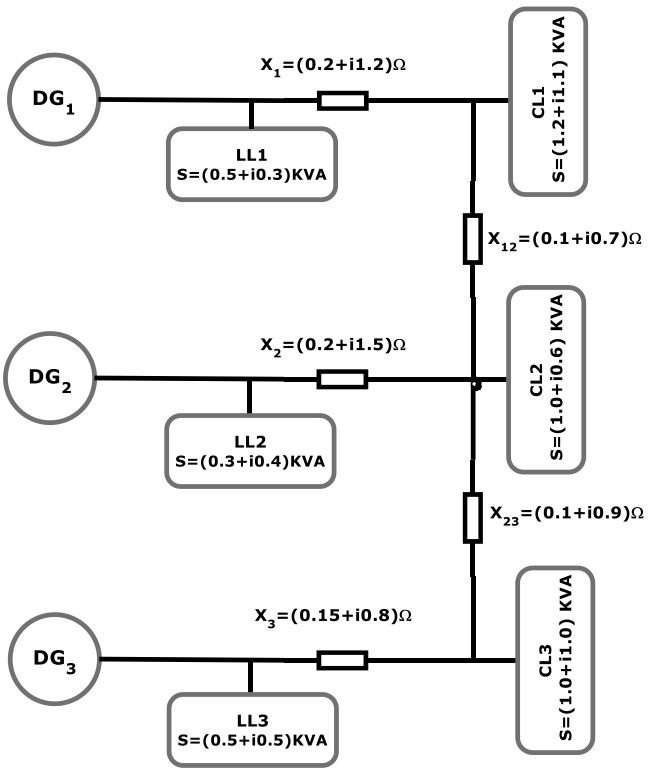


**Fig. 12.** Islanded microgrid with three distributed generators.

case, the local loads LL2 and LL3 together with the common loads CL1 and CL3 are connected, while the total load demand is kept constant.

Fig. 13 depicts the virtual impedance together with the active and reactive powers. Here, at the beginning of the simulation, during the period [0–0.5 s], the microgrid operates with a conventional droop control technique. On the contrary, during the period [0.5–2.5 s] the microgrid is controlled using a droopless method. Fig. 13(a) reveals a better share of the reactive power sharing for the droopless method. However, the error is still important. Fig. 13(c) shows that the both the controllers do not affect much the share of active power.

With reference to Fig. 14, during the period [0.5–2.5 s] the control of the microgrid has been enhanced with the introduction of the iterative adaptive virtual impedance. In this case, the adaptation coefficient has been set to 0.0012 that is half of the one used in the case of the droopless controller. Fig. 14(a) clearly shows the capability of the proposed method to obtain a perfect share of the reactive power in the microgrid.

The impedance mismatch is always present in the case of the droopless control because it introduces big values of virtual impedances, while for the proposed control technique the impedance mismatch is negligible as shown in Fig. 13(b) and Fig. 14(b).

Fig. 14(c) shows that as for the other methods, also the IAVI controller does not have a significant effect on the share of the active power.

### 5.2. Case study 2

In order to assess the dynamic behaviour of the proposed control strategy, the IAVI controller has been tested considering a variable reactive power demand. During the period [0–0.5 s], the system operates using a droop control, and the total reactive power demand is kept constant and equal to 2.9 kVAR. The local

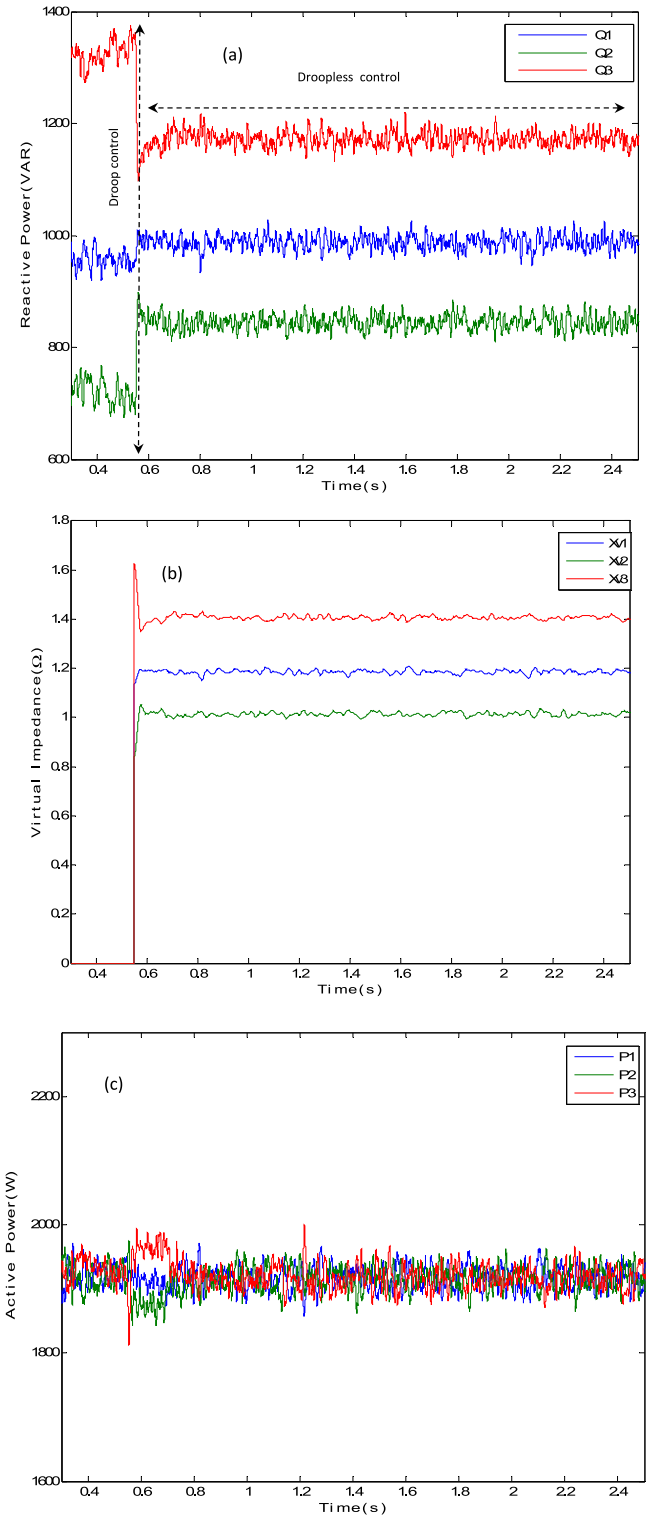


**Fig. 13.** Case study 1 — droopless and droop controllers: (a) reactive power, (b) virtual impedance, (c) active power.

load LL1 and the common load CL2 are disconnected, while all the other loads are connected.

During the period [0.5–4.5 s], the drop control is replaced by the IAVI controller, and the reactive power together with the configuration of the microgrid remain unchanged. During the period [4.5–7.5 s] the common load CL1 is added, and during the period [7.5–10.5 s] the local load LL1 is connected too. Finally,

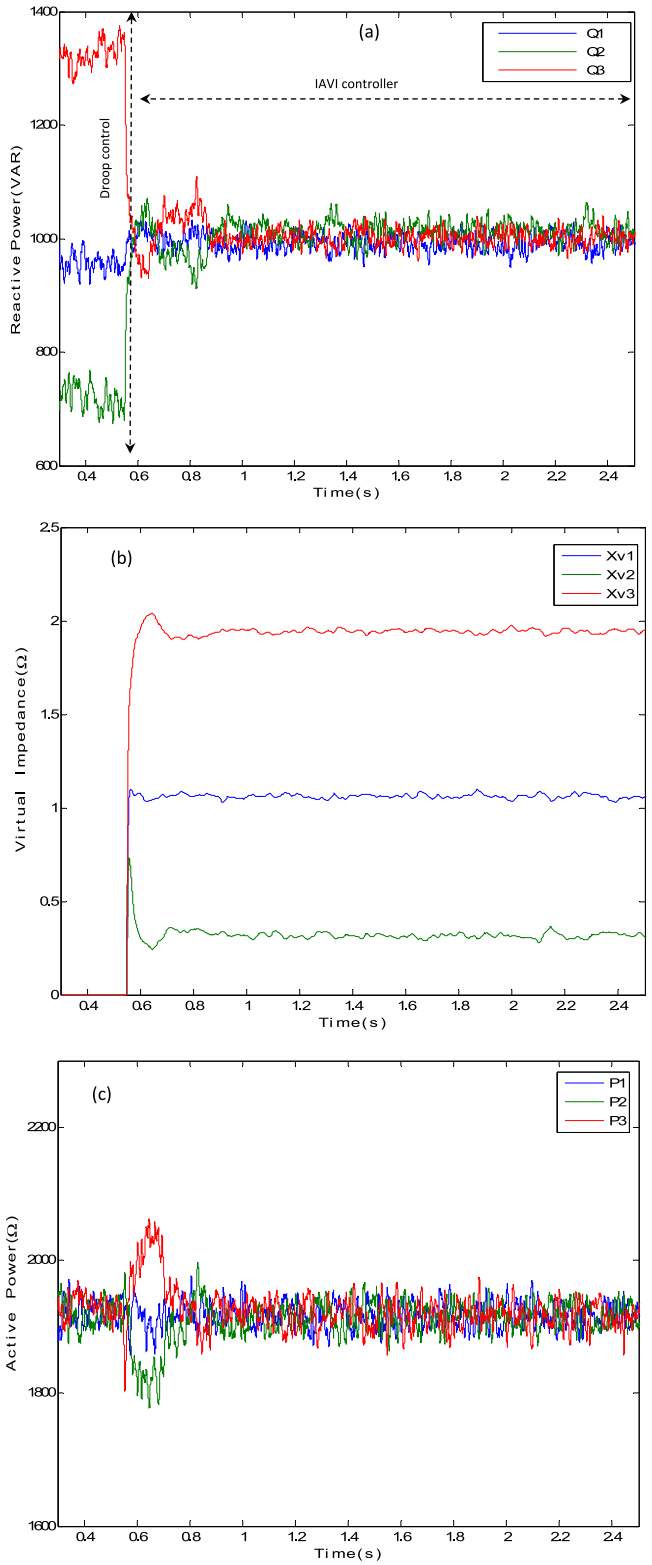


**Fig. 14.** Case study 1 — IAVI controller: (a) reactive power, (b) virtual impedance, and (c) active power.

during the period [10.5–13.5 s] the total amount of the reactive power demand is reduced to the 15% of the initial request.

Fig. 15(a) reveals that the designed IAVI controllers maintain an optimal reactive power sharing during all the considered intervals of time thanks to the adaptation of the virtual impedances that is shown in Fig. 15(b).

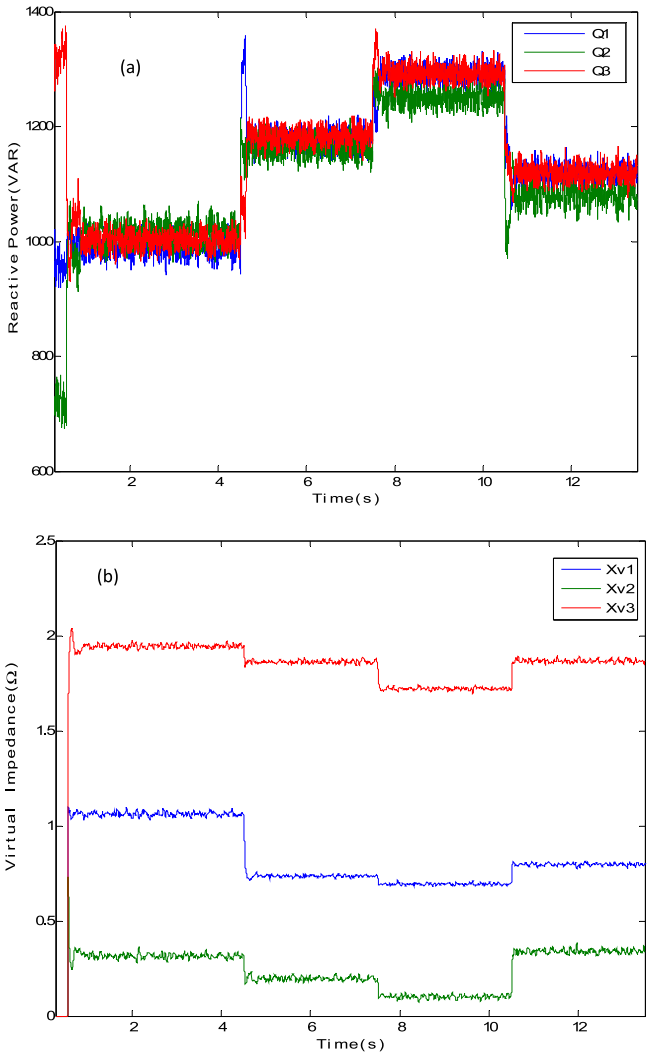


**Fig. 15.** Case study 2 (a) reactive power and (b) virtual impedance.

### 5.3. Case study 3

In order to evaluate the effect of the IAVI coefficients on the reactive power sharing, the operations of the microgrid depicted in Fig. 12 have been simulated for three different cases. Fig. 16(a) and Fig. 16(b) show that when the dominant poles are real, the share of the reactive power is always acceptable despite the value of coefficient $k_1$ is changed. On the contrary, Fig. 16(c) shows that when the dominant poles are complex, the sharing of reactive power is less accurate. This fact is due to the oscillations in the system response, which do not allow the IAVI controller to receive the true values of the variations in the reactive power.

## 6. Conclusion and future work

In this paper, an iterative adaptive virtual impedance (named IAVI) control strategy for the elimination of the mismatch between the impedances of the feeders in a meshed microgrid powered by a certain number of distributed generators has been presented.

The iterative virtual impedance consists of two elements: one proportional to the reactive power delivered by each generator, and a second that depends on the reactive power variation between two iterations. The proposed strategy is of particular

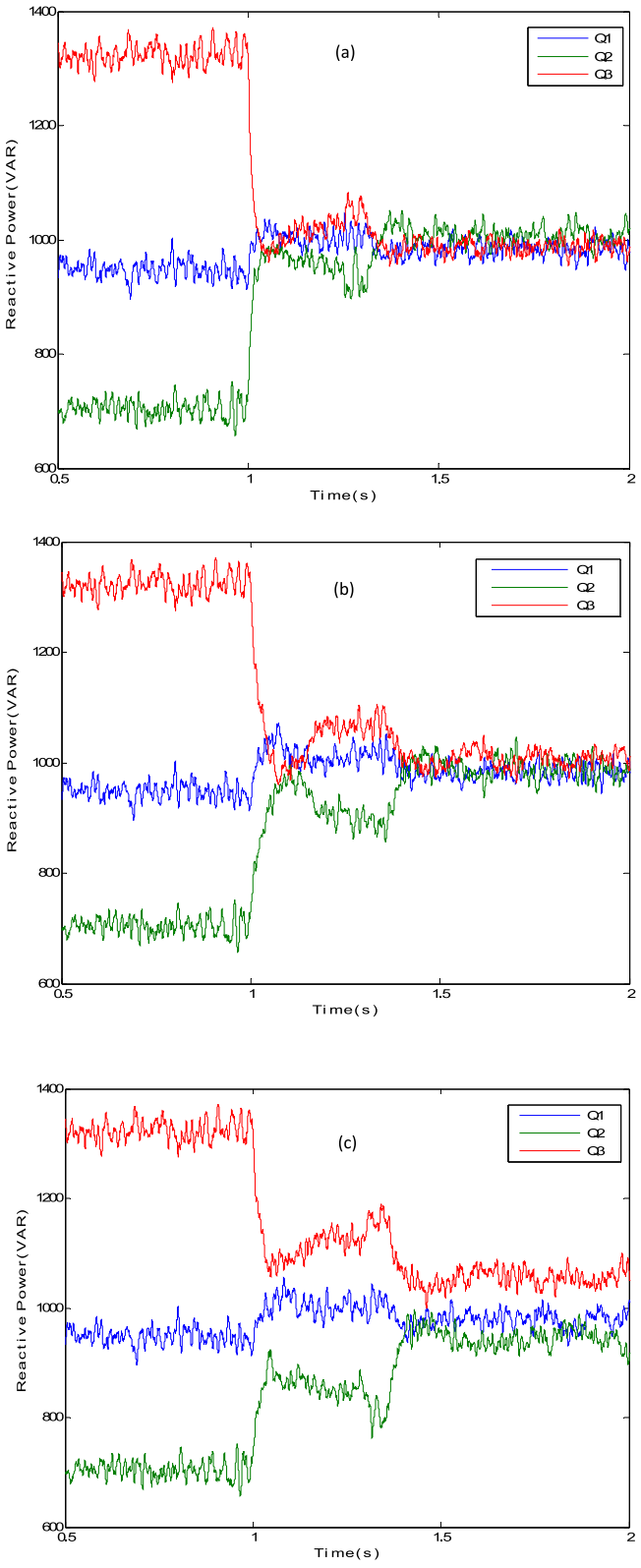


**Fig. 16.** Case study 3: (a) $k_1 = 0.0012$ and $\tau = 0.2$ s/VAR, (b) $k_1 = 0.008$ and $\tau = 0.2$ s/VAR, (c) $k_1 = 0.0012$ and $\tau = 0.3$ s/VAR.

interest as it does not need any communication link between the generators in the microgrid.

The behaviour of the IAVI controller has been simulated in a Matlab/Simulink environment, and the results show that the IAVI controller outperforms one of the most used control techniques such as the droopless one.

In addition, the method showed that the error in the share of the reactive power can be eliminated with a large margin of stability.

Further work will focus on the experimental verification of the proposed controller. In addition, in order to completely eliminate the dependence on the operating point, metaheuristic methods (such as ant colony optimization, particle swarm optimization, and genetic algorithm) will be used to accurately adjust the controller parameters.

## CRediT authorship contribution statement

**H. Sellamna:** Developed the theory and performed the computations, Verified and analysed the method, Written the paper. **A. Massi Pavan:** Conceived of the presented idea, Written the paper, Disused the results, Checked and revised the paper. **A. Mellit:** Conceived of the presented idea, Verified and analysed the method, Supervised the finding of this work, Written the paper, Disused the results. **Josep M. Guerrero:** Checked and revised the paper.

## Declaration of competing interest

The authors declare that they have no known competing financial interests or personal relationships that could have appeared to influence the work reported in this paper.

## Acknowledgements

A. Mellit would like to thank the International Centre for Theoretical Physics (ICTP), Trieste (Italy) for providing the materials and the computer facilities used to develop some parts of the work presented in the paper. A. Massi Pavan acknowledges the financial support provided by "DEEP-SEA – Development of energy efficiency planning and services for the mobility of Adriatic Marinas", a project co-financed by the European Regional Development Fund (ERDF) via the cross-border cooperation programme Interreg Italy-Croatia. J. M. Guerrero was supported by VILLUM FONDEN under the VILLUM Investigator Grant (no. 25920): Center for Research on Microgrids (CROM); www.crom.et.aau.dk.

## References

[1] M. Khederzadeh, H. Maleki, V. Asgharian, Frequency control improvement of two adjacent microgrids in autonomous mode using back to back Voltage-Sourced Converters, Int. J. Electr. Power Energy Syst. 74 (2016) 126–133.
[2] H. Seyed Mehdi, A. Hasankhani, M. Shafie-khahdJoão, P.S. Catalão, Demand response method for smart microgrids considering high renewable energies penetration, Sustain. Energy Grids Netw. (2020) 100325.
[3] Y. Sun, C. Zhong, X. Hou, J. Yang, H. Han, J.M. Guerrero, Distributed cooperative synchronization strategy for multi-bus microgrid, Int. J. Electr. Power Energy Syst. 86 (2017) 18–28.
[4] M. Hidehito, M.S. Kinjob-Shriram, R.G. Ramanathana, A.M. Hemeidad, T. Senjyu, Islanding operation scheme for DC microgrid utilizing pseudo Droop control of photovoltaic system, Energy Sustain. Dev. 55 (2020) 95–104.
[5] S.D. Tavakoli, M. Mahdavytakhr, M. Hamzeh, K. Sheshyekani, E. Afjei, et al., A unified control strategy for power sharing and voltage balancing in bipolar DC microgrids, Sustain. Energy Grids Netw. 11 (2017) 58–68.
[6] Z. Lyu, Q. Wei, Y. Zhang, J. Zhao, E. Manla, Adaptive virtual impedance droop control based on consensus control of reactive current, Energies 11 (7) (2018) 1801.
[7] Y. Li, Y.W. Li, Power management of inverter interfaced autonomous microgrid based on virtual frequency-voltage frame, IEEE Trans. Smart Grid 2 (1) (2011) 30–40.
[8] C.T. Lee, C.C. Chu, P.T. Cheng, A new droop control method for the autonomous operation of distributed energy resource interface converters, IEEE Trans. Power Electron. 28 (2013) 1980–1993.

[9] J. He, Y.W. Li, An enhanced micro-grid load demand sharing strategy, IEEE Trans. Power Electron. 27 (2012) 3984–3995.
[10] J.M. Guerrero, L.G. de Vicuna, J. Matas, M. Castilla, J. Miret, A wireless controller to enhance dynamic performance of parallel inverters in distributed generation systems, IEEE Trans. Power Electron. 19 (5) (2004) 1205–1213.
[11] J. He, Y.W. Li, J.M. Guerrero, F. Blaabjerg, J.C. Vasquez, An islanding microgrid power sharing approach using enhanced virtual impedance control scheme, IEEE Trans. Power Electron. 28 (11) (2013) 5272–5282.
[12] H. Mahmood, D. Michaelson, J. Jiang, Reactive power sharing in islanded microgrids using adaptive voltage droop control, IEEE Trans. Smart Grid 6 (6) (2015) 3052–3060.
[13] H. Han, Y. Liu, Y. Sun, M. Su, J.M. Guerrero, An improved droop control strategy for reactive power sharing in islanded microgrid, IEEE Trans. Power Electron. 30 (6) (2015) 3133–3141.
[14] C. Dou, M. Lu, T. Zhao, Decentralised coordinated control of microgrid based on multi-agent system, IET Gener. Transm. Dist. 9 (16) (2015) 2474–2484.
[15] J. Schiffer, T. Seel, J. Raisch, T. Sezi, Voltage stability and reactive power sharing in inverter-based microgrids with consensus-based distributed voltage control, IEEE Trans. Control Syst. Technol. 24 (1) (2016) 96–109.
[16] H. Sellamna, A. Mellit, A. Rabhi, H. Bekkay, B. Oral, Microgrid reactive power sharing using adaptive virtual impedance, in: Proc. of the IEEE International Conference on Wireless Technologies, Embedded and Intelligent Systems (WITS) Fez, Morocco, 2019.
[17] J.M. Guerrero, L.G. De Vicuna, J. Matas, M. Castilla, Miret, Output impedance design of parallel connected UPS inverters with wireless load-sharing control, IEEE Trans. Ind. Electron. 52 (4) (2005) 1126–1135.
[18] C. Dou, Z. Zhang, D. Yue, M. Song, Improved droop control based on virtual impedance and virtual power source in low-voltage microgrid, IET Gener. Transm. Dist. 11 (4) (2017) 1046–1054.
[19] P. Sreekumar, V. Khadkikar, A new virtual harmonic impedance scheme for harmonic power sharing in an islanded microgrid, IEEE Trans. Power Deliv. 31 (3) (2016) 936–945.
[20] Y. Zhu, F. Zhuo, F. Wang, B. Liu, Y. Zhao, A wireless load sharing strategy for islanded microgrid based on feeder current sensing, IEEE Trans. Power Electron. 30 (2015) 6706–6719.
[21] J. He, Y.W. Li, J.M. Guerrero, F. Blaabjerg, J.C. Asquez, An islanding microgrid power sharing approach using enhanced virtual impedance control scheme, IEEE Trans. Power Electron. 28 (2013) 5272–5282.
[22] H. Mahmood, D. Michaelson, J. Jiang, Accurate reactive power sharing in an islanded microgrid using adaptive virtual impedances, IEEE Trans. Power Electron. 30 (2015) 1605–1617.
[23] H. Sellamna, N. Rouibah, A. Mellit, G.M. Tina, H. Bekkay, Power flow control in autonomous micro-grid operation using ants colony optimization under variable load conditions, in: Proc. of the International Conference on Electronic Engineering and Renewable Energy Springer, Singapore, 2018, pp. 392–398.
[24] H. Yalong, X. Ji, P. Yonggang, Y. Pengcheng, W. Wei, Decentralised control for reactive power sharing using adaptive virtual impedance, IET Gener. Transm. Dist. 12 (5) (2018) 1198–1205.
[25] J. He, Y. Li, J.M. Guerrero, F. Blaabjerg, J.C. Vasquez, An islanding microgrid power sharing approach using enhanced virtual impedance control scheme, IEEE Trans. Power Electron. 28 (11) (2013) 5272–5282.
[26] Kim Sunghyok, Songchol Hyon, Chonung Kim, Distributed virtual negative-sequence impedance control for accurate imbalance power sharing in islanded microgrids, Sustain. Energy Grids Netw. 16 (2018) 28–36.
[27] H. Han, X. Hou, J. Yang, J. Wu, M. Su, J.M. Guerrero, Review of power sharing control strategies for islanding operation of AC microgrids, IEEE Trans. Smart Grid 7 (1) (2015) 200–215.
[28] J.A. Peças Lopes, C.L. Moreira, A.G. Madureira, Defining control strategies for microgrids islanded operation, IEEE Trans. Power Syst. 21 (2) (2006) 916–924.
[29] J. Rocabert, A. Luna, F. Blaabjerg, P. Rodriguez, Control of power converters in AC microgrids, IEEE Trans. Power Electron. 27 (11) (2012) 4734–4749.